Electronic and dielectric properties of insulating Zr_3N_4

W. Y. Ching, Yong-Nian Xu, and Lizhi Ouyang
Department of Physics, University of Missouri-Kansas City, Kansas City, Missouri 64110
(Received 17 July 2002; revised manuscript received 1 October 2002; published 13 December 2002)

The electronic structures and dielectric functions of Zr_3N_4 were studied by a first-principles density-functional method. Three different structure models were used: (1) ZrN in a rocksalt structure with an ordered Zr vacancy, or $Zr_3\square N_4$, (2) c-Zr_3N_4 in the cubic spinel structure and (3) o-Zr_3N_4 in the orthorhombic structure. All three structures of Zr_3N_4 are found to be insulators with small indirect band gaps. This appears to be consistent with experimental observation that Zr_3N_4 is an insulator. Total-energy (E) calculations show that $Zr_3\square N_4$ has an expanded lattice constant compared to ZrN by about 0.75%, and that $E(Zr_3\square N_4) < E(o\text{-}Zr_3N_4) < E(c\text{-}Zr_3N_4)$ which indicates that the ordered defect model for Zr_3N_4 is valid. It is further demonstrated that past calculations showing $Zr_3\square N_4$ to be a metal were caused by the failure to relax the vacancy structure. The electronic structures and the optical dielectric functions for all three models were calculated and analyzed in detail. The $Zr_3\square N_4$ model again shows the best overall agreement with available experimental data. All three structures have relatively large optical dielectric constants at zero frequency. Possible implications from these calculations are discussed.

DOI: 10.1103/PhysRevB.66.235106 PACS number(s): 78.66.Nk

I. INTRODUCTION

ZrN is a refractory material with many outstanding physical properties such as high melting temperature, high hardness, and resistance to radiation. ZrN is also a superconductor with a transition temperature T_c of 10 K.[1] Very recently, it was found that the layered compounds ZrNCl and Li_xZrNCl are also superconductors with a higher T_c of 13 and 25.5 K respectively.[2,3] The electronic structure of ZrN in the rocksalt structure is well known [4–6]. Its metallic band structure is manifested in the golden color of the crystal itself. In contrast, Zr_3N_4 is an insulator. It was first discovered by Juza *et al.* who showed it to be semitransparent with a brownish color.[7] In the preparation of ZrN_x thin films by chemical vapor deposition (CVD) or physical vapor deposition (PVD) using a dual ion-beam splitting technique, it was clearly demonstrated that stochiometric Zr_3N_4 exists in the N-rich limit.[8,9] Photoemission and optical data on ZrN_x films show dramatic changes from $x=1$ to $x=1.3333$,[10] strongly supporting the existence of a metastable and insulating compound, Zr_3N_4. In contrast, Ti_3N_4 films were found to be metallic with a golden color.[9]

The exact structure of Zr_3N_4 is not known. However, it is generally believed that Zr_3N_4 is closely related to ZrN in the rocksalt structure with a Zr vacancy. We denote this defect model as $Zr_3\square N_4$. The combination of a superconducting ZrN and an insulating Zr_3N_4 raised an interesting possibility of fabricating a Josephson junction based on a $ZrN/Zr_3N_4/ZrN$ superlattice.[11,12] Since ZrN and Zr_3N_4 are isostructural and isochemical, there will be very little interface effects at the metal-insulator interface. Such a junction could significantly enhance the superconducting tunneling effect. Unfortunately, practical applications of such a Josephson junction have not been realized in spite of intense research efforts more than a decade ago.[8,11,12] In connection with the search for the $ZrN/Zr_3N_4/ZrN$ junction, the electronic structure of Zr_3N_4 was investigated. Schwarz *et al.* [12] had calculated the band structure of $Zr_3\square N_4$ represented by the vacancy model of ZrN. Using the augmented spherical wave (ASW) method, they showed that the defect model of Zr_3N_4 is a metal, not an insulator. Several groups then attempted similar calculations with somewhat different approaches and reached similar conclusion.[13,14] The apparent contradiction with the experimental observation[8–10] was rationalized by two possibilities. (1) The underlying electronic structure theory based on local density approximation (LDA) of the density-functional theory is somehow not suitable for Zr_3N_4; (2) the defect model for Zr_3N_4 is not the correct model and there may be hitherto undiscovered crystalline phases of Zr_3N_4 that should be more appropriate.

In 1996, Lerch and co-workers reported the synthesis of crystalline Zr_3N_4 and determined its structure by x-ray powder diffraction.[15] Zr_3N_4 was reported to have an orthorhombic structure with a space group of either *Pnam* or $Pna2_1$ with four formula units per unit cell. Further analysis of the diffraction data indicated that the assignment of the space group *Pnam* was the appropriate one.[16] We will refer to this crystalline phase as o-Zr_3N_4. In o-Zr_3N_4, there are three nonequivalent types of Zr (Zr1, Zr2, Zr3) and four nonequivalent types of N (N1, N2, N3, N4).[15] Zr1 is octahedrally coordinated to six N. Zr2 is at the center of a triangular prism with another N at a slightly larger distance away (Zr2-N2 = 2.74 Å). Zr3 is in a heavily distorted octahedron with yet another N not too far away (Zr3-N3 = 2.94 Å). So, Zr2 and Zr3 in o-Zr_3N_4 can be considered sevenfold bonded which accounts for its relatively high density. Because of the complexity of the crystal structure, no electronic structure on o-Zr_3N_4 has been attempted.

Very recently, we have suggested that Zr_3N_4 might exist in the cubic spinel phase (denoted by c-Zr_3N_4) similar to c-Si_3N_4.[17] The successful synthesis of the spinel phase of Si_3N_4 at high temperature and pressure[18] in addition to the well-known hexagonal phases of Si_3N_4 (the α and β phases) was a recent surprises in materials synthesis since octahedral

TABLE I. Comparison of the crystal structures of $Zr_3\square N_4$, c-Zr_3N_4 and o-Zr_3N_4.

Crystal model	$Zr_3\square N_4$	c-Zr_3N_4	o-Zr_3N_4
Structure	Simple cubic	Spinel	Orthorhombic
Lattice constants (Å)	$a=4.596$	$a=9.1185$	$a=9.7294$
		$u=0.3829$	$b=3.28$
			$c=10.8175$
Space Group	no symmetry	Fd3m	Pnam
Z	1	2	4
Vol/FU (Å^3)	97.08	94.85	86.25
Density (gm/cc)	5.63	5.77	6.34

bonding for group-IV elements such as Si is quite unusual. Since then, several laboratories have verified the existence of c-Si_3N_4, c-Ge_3N_4 and c-Sn_3N_4.[19–24] This has spurred a flurry of research activities on the possibilities of spinel nitrides formed by both group-IV A and group-IV B elements.[17,25–28] In particular, it was reported that c-Ti_3N_4 and c-Zr_3N_4 could both exist based on theoretical modeling.[27] Electronic structure calculations using the predicted structures showed c-Ti_3N_4 to be a metal and c-Zr_3N_4 to be an insulator with a small indirect band gap.[27,28]

In this paper, we present a detailed study of the electronic structure and optical properties of Zr_3N_4 based on the three different structural models. (1) The ordered defect model of $Zr_3\square N_4$ similar to past studies, except in the present case, the defect structure is fully relaxed. (2) c-Zr_3N_4 in the spinel structure and (3) the orthorhombic o-Zr_3N_4. Figure 1 shows the three structural models for Zr_3N_4. The crystal parameters are summarized in Table I. The crystal parameters for c-Zr_3N_4 are the theoretical predicted values using a total-energy minimization scheme.[29,30] The main goal of our study is to compare and contrast the electronic structures of different models of Zr_3N_4. By comparing the calculated physical properties with experimental observations, the most appropriate structure model for Zr_3N_4 can be identified. We show that although all three structures have an insulating band structure, the ordered defect model is the most consistent with the overall experimental observations, and as such, should be regarded as the correct structure for Zr_3N_4 at low temperature and ambient pressure. We further investigate as to why the past calculations on the defect model produced a metallic band for $Zr_3\square N_4$.

The organization of this paper is as follows. In the following section, we briefly outline the method of our calculation. The results of the electronic structure and optical properties of the three models are presented in Sec. III. These results are compared and discussed in Sec. IV. Some conclusions are drawn in last Sec. V.

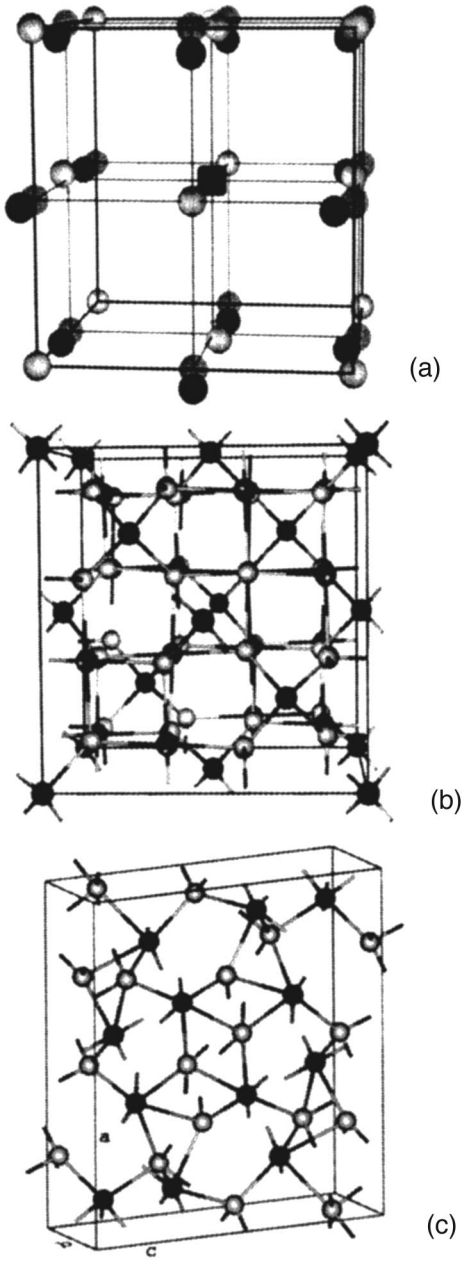

FIG. 1. The crystal structures of three models used in the present calculation: (a) The fully relaxed ordered defect model $Zr_3\square N$, (b) the cubic spinel model c-Zr_3N_4 and (c) the orthorhombic o-Zr_3N_4. Dark balls represent Zr atoms and light balls N atoms. The solid square in (a) denotes the Zr vacancy.

II. METHOD OF CALCULATION

The electronic structures of the Zr_3N_4 models were calculated using the orthogonalizaed linear combination of atomic orbital (OLCAO) method.[31] The OLCAO method is a density-functional theory-based all-electron method that is particularly effective for crystals with complex structures such as c-Zr_3N_4 and o-Zr_3N_4. The method has been successfully applied to many different types of complex crystals[32–36] with accuracy comparable to any other *ab initio* electronic structure methods. In the present calculation, a full basis set consisting of atomic orbitals of Zr ([Kr] core plus Zr-5s, 6s, 5p, 6p, 4d, 5d) and N ([He] core plus N-2s, 3s, 2p, 3p) was adopted. The total energy of the crystal was calculated based on LDA theory with all internal parameters fully relaxed.[29,30] As a preliminary test, the band structure

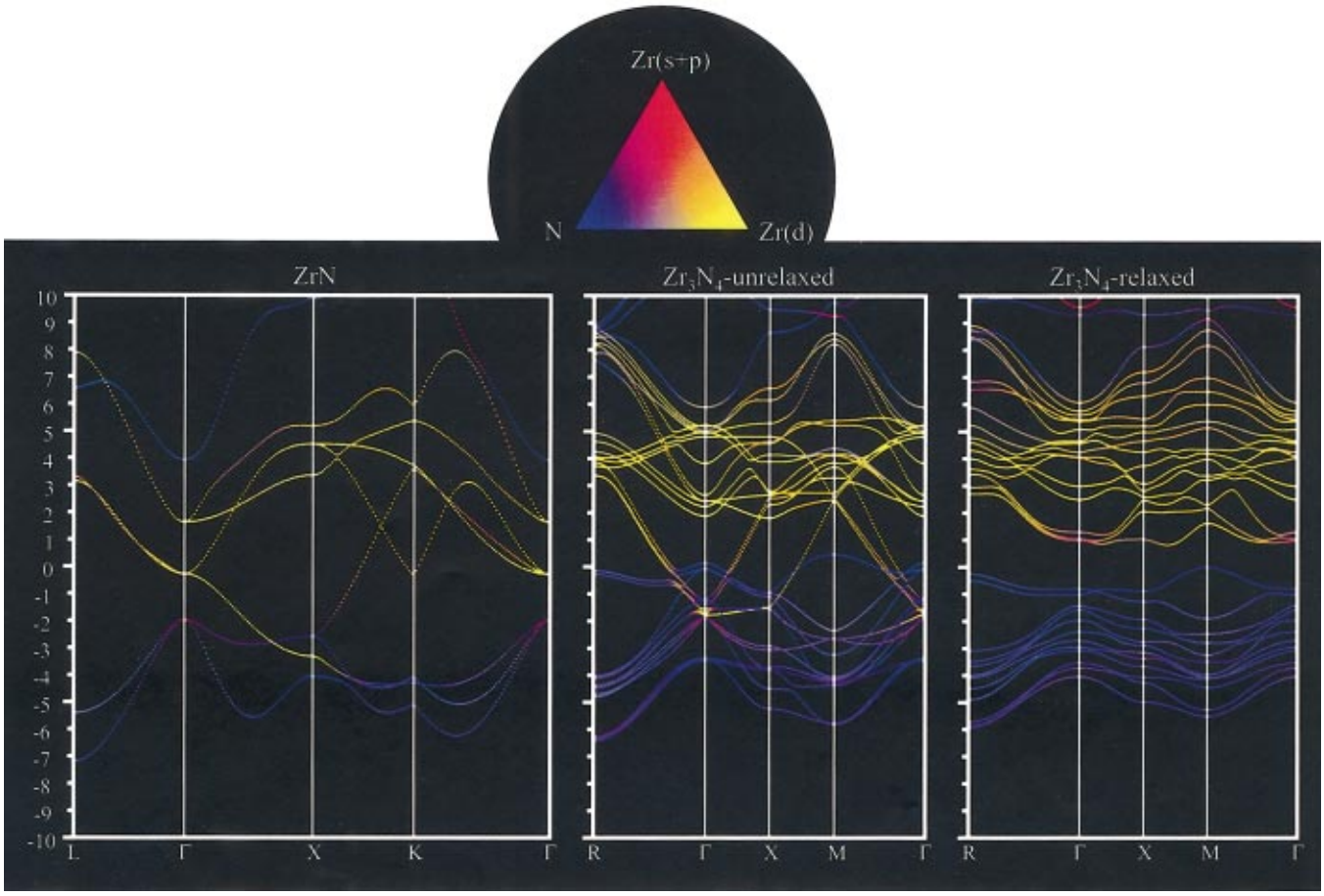

FIG. 2. (Color) Band structure of (a) ZrN in the rocksalt structure (left panel); (b) unrelaxed $Zr_3\square N_4$ (middle panel); and (c) relaxed $Zr_3\square N_4$ (right panel). The upper triangle shows the color code due to the mixing of the wave functions. Red, Zr $(s+p)$ orbitals; yellow, Zr-4d orbitals, and blue, N orbitals.

and density of states (DOS) of ZrN in the rocksalt structure were calculated and shown in Fig. 2(a) and Fig. 3(a), respectively. Its metallic band is in full agreement with the existing LDA calculations by Stampfl *et al.*[4] and Schwarz *et al.*[5]

The calculation of the dielectric function follows the theory of interband transitions with all dipole matrix elements included. To achieve higher accuracy for wave functions at higher-energy ranges, the all-electron secular equations without orthogonalization were solved. Large numbers of k points in the Brillouin zone (BZ) integration were used to ensure sufficient convergence (102 k points for $Zr_3\square N_4$, 110 k points of c-Zr_3N_4 and 72 k points for o-Zr_3N_4 in the irreducible portions of the BZ). Test calculations with different numbers of k points indicate that this level of k-point sampling is adequate. The imaginary parts of the dielectric functions $\varepsilon_2(\omega)$ were calculated first. The real parts $\varepsilon_1(\omega)$ were obtained from the imaginary parts by Kramers-Kronig conversion. The energy-loss functions were obtained from the inverse of the complex dielectric function, or $\mathrm{Im}[[\varepsilon_1(\omega)+i\varepsilon_2(\omega)]^{-1}]$.

The bulk properties of the three models of Zr_3N_4 were obtained by fitting the calculated total energy vs volume data to the Murnagham equation of state (EOS).[37] For each fixed volume, all the internal parameters of c-Zr_3N_4 and o-Zr_3N_4 were fully relaxed. For $Zr_3\square N_4$, all the seven atoms in the

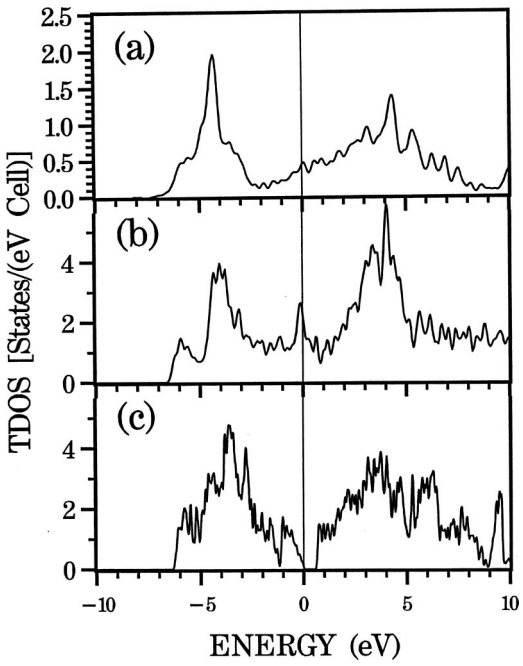

FIG. 3. DOS of (a) ZrN in the rocksalt structure; (b) unrelaxed $Zr_3\square N_4$; and (c) relaxed $Zr_3\square N_4$.

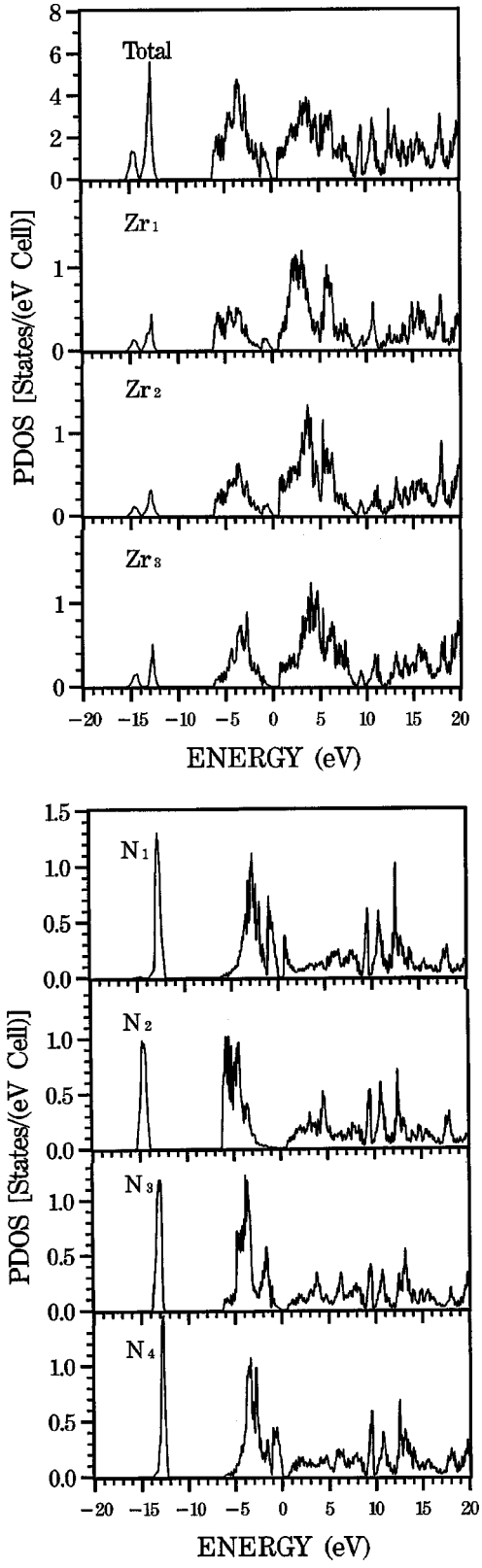

FIG. 4. Total DOS and PDOS of relaxed $Zr_3\square N_4$.

cubic cell were relaxed until the total energy per cell converged to the order of 0.0005 eV per cell.

One of the special advantages of the OLCAO method is the ease with which the Mulliken effective charge Q_α^* on each atom and the bond order (BO), $\rho_{\alpha,\beta}$ between pairs of nearest-neighbor atoms α and β (also called the overlap population) can be obtained.[38] This scheme provides a simple, effective, and unbiased assessment of the charge transfer and overall bonding picture in a crystal. It is customary to use a minimal basis set for the effective charge and bond order calculations. The Q_α^* and $\rho_{\alpha\beta}$ are defined by the following equations:

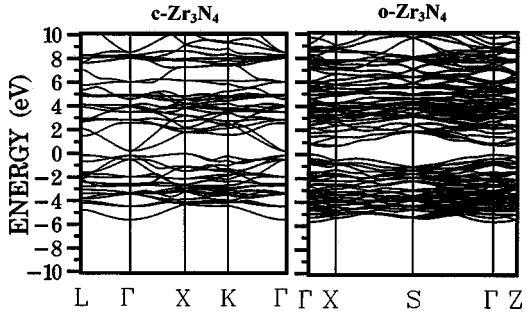

FIG. 5. Band structure of c-Zr_3N_4 (left panel), o-Zr_3N_4 (right panel).

$$Q_\alpha^* = \sum_i \sum_{n,occ} \sum_{j,\beta} C_{i\alpha}^{*n} C_{j\beta}^n S_{i\alpha,j\beta}, \tag{1}$$

$$\rho_{\alpha\beta} = \sum_{n,occ} \sum_{i,j} C_{i\alpha}^{*n} C_{j\beta}^n S_{i\alpha,j\beta}, \tag{2}$$

where $C_{i\alpha}^n$ is the coefficient of the eigenvector of the nth band. α specifies the atom and i denotes the orbital. $S_{i\alpha,j\beta}$ is the overlap matrix between the Bloch functions.

III. CALCULATED RESULTS

A. Electronic structure

Before we present the electronic structure result for the defect model $Zr_3\square N_4$, we first investigate why the past calculations[12] on $Zr_3\square N_4$ showed it to be metallic. We have repeated such a calculation without the internal relaxation of the atoms in the vacancy model using the OLCAO method. The resulting band structure and the DOS are shown in Figs. 2(b) and 3(b), respectively. It clearly shows that such a calculation indeed results in a metallic band structure and that the calculated DOS is in very close agreement with that of Schwartz *et al.* using the ASW method.[12] In Ref. 12, the equilibrium lattice constant obtained for $Zr_3\square N_4$ is smaller than that of ZrN by 1.5%, which is inconsistent with the experimental data.[9] In our relaxed calculation, the lattice constant of $Zr_3\square N_4$ expands by 0.75% over ZrN.

In Fig. 2(c) and Fig. 3(c), we show the band structure and DOS of $Zr_3\square N_4$ with all the atoms in the cubic cell fully relaxed in response to the presence of the Zr vacancy. As illustrated in Fig. 1(a), there are significant movements of the N and Zr atoms. In the unrelaxed model, the Zr-N bond lengths are 2.298 Å. After relaxation, the Zr-N bonds range from 1.979 to 2.672 Å. It is this relaxation effect and the slightly expanded lattice constant that have significantly affected the Zr-N interaction, resulting in the insulating band

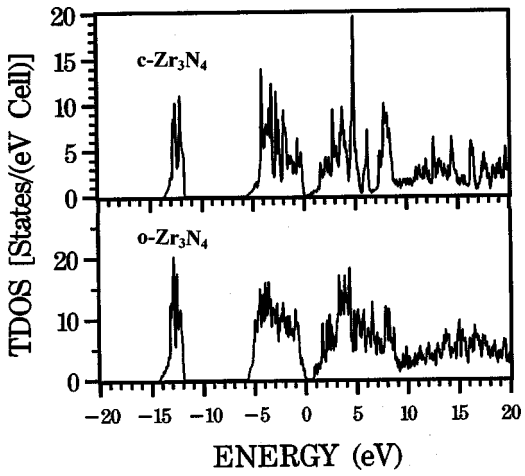

FIG. 6. Total DOS of c-Zr_3N_4 (upper panel) and o-Zr_3N_4 (lower panel).

structure for $Zr_3\square N_4$. The calculated indirect band gap is 0.82 eV and the direct band gap at Γ is 1.80 eV. The real band gap could be even larger since it is well known that the LDA calculation generally underestimates the band gap. Fix *et al.* had estimated the optical band gap of Zr_3N_4 thin film to be 2.2 eV.[9] However, this optical band gap was obtained by extrapolating the absorption coefficient α, which had not been corrected for interference effects, and therefore has a large degree of uncertainty.

In order to vividly show the hybridization between N orbitals and the Zr $(s+p)$ and Zr-4d orbitals, we plot the band structures of ZrN, $Zr_3\square N_4$ (unrelaxed) and $Zr_3\square N_4$ (relaxed) in color code in Fig. 2. That plot clearly shows that the metallization of ZrN in the rocksalt structure arises from the Zr-4d bands. One such band along the Γ-X direction

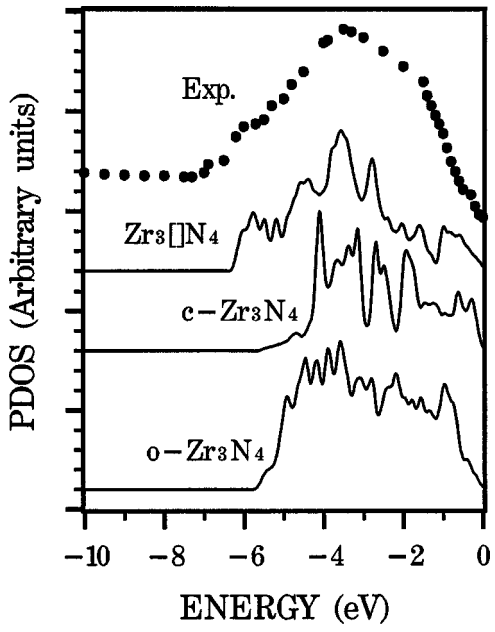

FIG. 7. Comparison of the upper valence band DOS of (a) $Zr_3\square N_4$, (b) c-Zr_3N_4 and o-Zr_3N_4 (c) with the experimental XPS data of Ref. 10 (dotted line).

TABLE II. Comparison of the measured and relaxed crystal parameters in o-Zr_3N_4. The relaxed values are shown in parentheses.

Lattice constants (Å)	$a=9.7294$ (9.5238) $b=3.281$ (3.2869) $c=10.8175$ (10.8654)		
Atom	x	y	z
Zr1	0.4316 (0.4279)	0.6241 (0.6210)	1/4
Zr2	0.3922 (0.3924)	0.0934 (0.0961)	1/4
Zr3	0.2671 (0.2614)	0.3519 (0.3490)	1/4
N1	0.238 (0.2275)	0.710 (0.7152)	1/4
N2	0.138 (0.1455)	0.984 (0.9841)	1/4
N3	0.999 (1.0085)	0.227 (0.2291)	1/4
N4	0.606 (0.6054)	0.024 (0.0226)	1/4

actually penetrates well below the Fermi level. In the relaxed $Zr_3\square N_4$ model a gap develops separating the valence bands (VB), which consist mostly of N-2p orbitals, from the conduction bands (CB), which consist of the hybridized s-d bands of Zr. Near the bottom of the CB, the Zr-s character becomes more prominent. In the unrelaxed case shown in Fig. 2(b), the separation of the VB and the CB is not complete. The Zr-4d bands interfere with the N bands resulting in the disappearance of the gap. It should be pointed out that our earlier calculation on a similarly relaxed defect model of $Ti_3\square N_4$ yielded a metallic band structure[17] in close agreement with experimental observation.[9]

In Fig. 4, we display the total and the atom-resolved partial DOS (PDOS) of the relaxed $Zr_3\square N_4$ model. As the result of atomic relaxation, the PDOS of the three Zr and four N atoms are quite different, especially the N atoms, reflecting the somewhat different local bonding environment for each atom.

Figures 5 and 6 show the calculated band structure and total DOS of c-Zr_3N_4 and o-Zr_3N_4, respectively. For c-Zr_3N_4, the top of the VB is at X and the bottom of the CB is at Γ with an indirect band gap of 0.22 eV. The direct band gap is 0.38 eV at Γ. The total DOS shows some resemblance to that of $Zr_3\square N_4$. The PDOS for Zr (not shown) at the tetrahedral site (Zr1) and the octahedral site (Zr2) show significant differences especially in the CB region, reflecting the difference in their bonding environments.

The calculated band structure of o-Zr_3N_4 shows that it has an indirect band gap of 0.71 eV. The top of the VB is at Γ and the bottom of the CB is at a point along Γ-Z. As mentioned earlier, the three Zr atoms and four N atoms in o-Zr_3N_4 occupy crystallographically inequivalent sites with very different local bonding structures. Such differences can be seen in the PDOS of each atom (not shown), especially for the N atoms in the VB region. For example, the spectral weight in the PDOS for N4 is at a higher binding energy mainly due to its shorter Zr-N bond lengths (Zr2-N4 $=2.07$ Å, Zr3-N4 $=2.06$ Å).

In Fig. 7, we display the broadened total DOS of the upper VB in the three models for Zr_3N_4, and compare them with the XPS data of Ref. 10. Clearly, the result of $Zr_3\square N_4$ (c-Zr_3N_4) agrees well with the experimental data best

TABLE III. Calculated bulk and optical parameters of $Zr_3\square N_4$, c-Zr_3N_4 and o-Zr_3N_4.

Crystal model	$Zr_3\square N_4$	c-Zr_3N_4	o-Zr_3N_4
Band gap (eV)	0.821 (indirect)	0.223 (indirect)	0.705 (indirect)
	1.800 (at Γ)	0.387 (at Γ)	0.83 (at Γ)
Band width (eV):			
Upper VB	5.9	5.6	5.7
Lower N-2s band	3.22	1.89	2.26
B (GPa)	298.9$\pm$30	226.5	238.3
B'		4.17	3.65
$\varepsilon_1(0)$	7.82	8.37	10.23
ω_p (eV)	12, 24, 32, 36.	12.5, 24, 33, 36.	11.5, 26, 33, 37
(Expt. peaks)	13, 22, 33, 40		
TE/FU	-1367.6925	-1364.702	-1365.3042
ΔE/FU (eV)	0.0	2.82	2.39

(least), not just in the width of the upper VB, but also in the shape of the DOS profile. c-Zr_3N_4 and o-Zr_3N_4 have narrower upper VB (5.6 and 5.7 eV, respectively) compared to that of $Zr_3\square N_4$ (5.9 eV).

B. Bulk properties

The total energies (E) of the three models were calculated at different volumes with all the internal parameters relaxed. The fully relaxed structural parameters for o-Zr_3N_4 are listed in Table II. For the $Zr_3\square N_4$ model, we find the equilibrium lattice constant to be slightly larger than that of ZrN in the rocksalt structure by 0.75%. This is consistent with the estimation of Fix *et al.*[9] that the lattice constant of "Zr_3N_4" phase in the CVD film is slightly larger than the lattice constants of ZrN. The bulk moduli and the pressure coefficients for all three model structures are obtained by fitting the calculated total energy vs volume data to the Murnagham equation of states (EOS).[37] At the equilibrium volume, it is shown that the total electronic energy per formula unit (FU) is lowest for $Zr_3\square N_4$ and highest for c-Zr_3N_4 with o-Zr_3N_4 being intermediate. The relative energy numbers are listed in Table III.

The bulk moduli of o-Zr_3N_4 and c-Zr_3N_4 are estimated from the EOS fits to be 238 and 225 GPa, respectively. The bulk modulus of $Zr_3\square N_4$ is much more difficult to obtain accurately because the defect model apparently has multiple local energy minima in the total-energy landscape making it very sensitive to variation in lattice constant. The bulk modulus of $Zr_3\square N_4$ is estimated to be in the range of 299 $\pm$20 GPa. It is a little surprising to see that $Zr_3\square N_4$ has the highest B value among the three crystals. In Fig. 8, we show the calculated E vs V data and the fitted curves for the three models. It is conceivable that $Zr_3\square N_4$ may be transformed to o-Zr_3N_4 by a suitable application of pressure. From the slope of the common tangent to the E vs V curves, we have roughly estimated the transition pressure P_t to be about 36 GPa. This value has to be treated with caution because of the larger uncertainty in the E vs V data in the case of $Zr_3\square N_4$. At an even higher pressure, transformation to the predicted spinel phase c-Zr_3N_4 cannot be ruled out. Most of the electronic and bulk properties of these three models are summarized in Table III.

C. Effective charges and bonding

It has been suggested that in ZrN compounds, all three types of bonding (metallic, covalent, and ionic) are present.[11] Since all three models of Zr_3N_4 yield an insulating band structure, the notion of metallic bonding in Zr_3N_4 can be discarded. The effective charge and bond-order calculation can reveal much of these crystals bonding characteristics. The calculated Mulliken effective charges Q_α^* and the BO values for the three Zr_3N_4 models are listed in Table IV, along with the interatomic distances. It can be seen that the average Q_α^* for Zr and N in the three models are not much different. On average, there is about 0.7 electron transferred from a Zr atom to the N atoms, much less than that implied

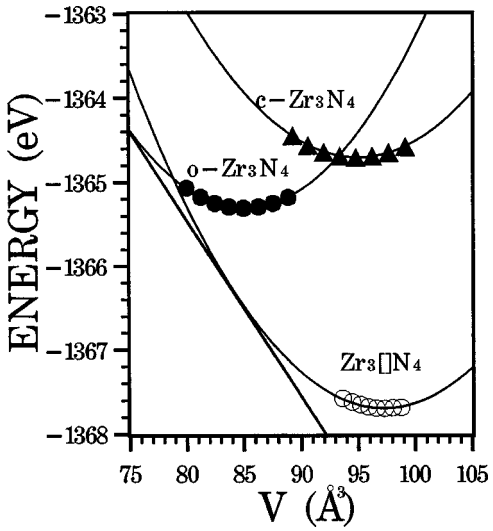

FIG. 8. The calculated total-energy unit vs volume (per formula unit) in the three models of Zr_3N_4. Solid symbols are the calculated data and the lines are the fitted EOS curves. The straight line is the common tangent.

TABLE IV. Calculated Mulliken effective charges and bond order in three models. The Zr-N bond lengths are listed in parentheses.

Crystal model	$Zr_3\square N_4$	c-Zr_3N_4	o-Zr_3N_4
Q^*_{Zr} (electron)	3.25, 3.31, 3.31	3.08(t), 3.29(o)	3.25, 3.22, 3.26
Q^*_N (electron)	5.52, 5.63, 5.50, 5.50	5.61	5.58, 5.59, 5.55, 5.55
Bond order (electron):			
Zr-N bond (BL in Å)	0.211 (2.312)	0.342 (2.101)	0.233 (2.213)
	0.211 (2.323)	0.246 (2.210)	0.192 (2.308)
	0.209 (2.324)		0.187 (2.376)
Average Zr-N BO	0.211	0.265	0.204
Total crystal BO (per formula unit)	3.784	4.718	4.052

by the formal valency of 4+ in the ionic description of the group-IV elements. Therefore, the ionic bonding picture in Zr_3N_4 compound is also less tenable. The nearest-neighbor BO values for the three models range from 0.19 to 0.34, much higher than those in the ionic oxides such as Al_2O_3 and $Y_3Al_3O_{12}$.[32] Thus, in Zr_3N_4, covalent bonding dominates. In c-Zr_3N_4, the Q^* for Zr at the tetrahedral site (Zr_{tet}) is less than the Q^* for Zr at the octahedral site (Zr_{oct}) because the former has a much shorter Zr-N bond. Because of the very short bond length of ZrI-N (2.10 Å) in c-Zr_3N_4, its BO of 0.34 is much larger than the BO of any other Zr-N pairs in the three crystals. If we consider the total BO per formula unit as a single parameter to measure the bond strength of a crystal, then clearly, c-Zr_3N_4 has the highest overall BO, hence it has the strongest covalent bonding.

D. Dielectric properties

In Figs. 9–11, we display the calculated dielectric functions and the energy-loss functions for $Zr_3\square N_4$, c-Zr_3N_4, and o-Zr_3N_4, respectively. The gross features of the spectra from the three models are quite similar. Subtle differences exist in the spectral region below 10 eV. In all three models, the absorption peaks in $\varepsilon_2(\omega)$ centered near 30 eV originate from the transitions from the shallow Zr-4p core levels. In o-Zr_3N_4, $\varepsilon_2(\omega)$ has a broad peak at 6.0 eV and a small but discernable peak at 1.5 eV above the absorption edge. There is another broad peak between 14 and 26 eV, which is present in all three models. In c-Zr_3N_4 and $Zr_3\square N_4$, the absorption structures in $\varepsilon_2(\omega)$ are much more complex with multiple peaks. For the $Zr_3\square N_4$ model, there is a sharp peak at 2.5 eV at the absorption edge that is not present in the other two models. Obviously, the differences in the absorption curves of the three models are intimately related to the differences in the direct and indirect band gaps, as well as the distributions of the occupied and unoccupied states in the three crystal models.

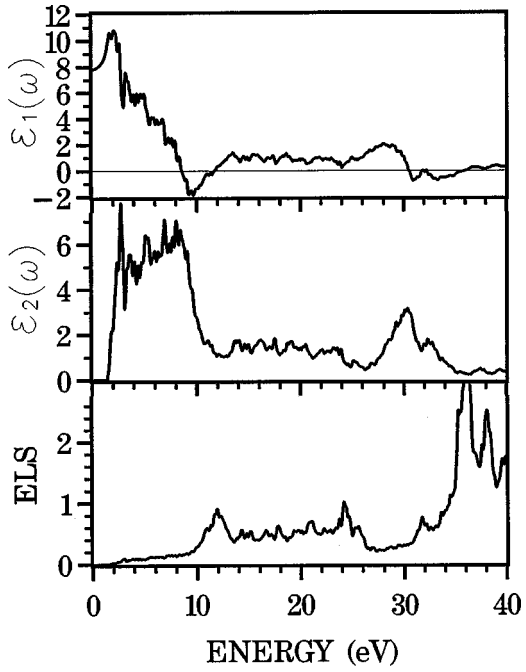

FIG. 9. Real (a) and imaginary (b) dielectric function, and energy-loss function (c) of $Zr_3\square N_4$.

The calculated optical dielectric constant $\varepsilon_0=\varepsilon_1(\hbar\omega=0)$ for the three crystals are found to be 7.82, 8.37, and 10.23, respectively. ε_0 can be related to the measured refractive index for Zr_3N_4 through $n=\sqrt{\varepsilon_0}$. Fix *et al.*[9] had estimated the refractive index for Zr_3N_4 films to be ranging from 2.9 to 3.3 while Camellio *et al.* had obtained a value of $n=2.55$,[39] for Zr_3N_4 films using ellipsometric measurements. As can be seen, these refractive index values are closer to the calculated $n=\sqrt{\varepsilon_0}$ value of 2.80 for $Zr_3\square N_4$, and less well matched with those of c-Zr_3N_4 and o-Zr_3N_4.

The peaks in the electron energy-loss function are interpreted as the energy for bulk-plasma excitation. There are multiple plasmon peaks in the calculated energy-loss spectra for all three models shown in part (c) of Figures 9–11. The calculated spectra at the higher-energy region (>26 eV) are less reliable. The values of plasmon peaks ω_p in eV are listed in Table IV. Concentrating on $Zr_3\square N_4$, we can roughly identify plasmon peaks at 12, 24, 32, and 36 eV. The spectra for o-Zr_3N_4 and c-Zr_3N_4 are similar with slight changes in peak positions and amplitudes. Prieto *et al.* measured the dielectric properties of Zr, ZrN, Zr_3N_4, and ZrO_2 using reflection electron energy-loss spectroscopy.[40] By modeling the measured inelastic scattering cross section with a mathematical model, they have converted the data to the energy-loss function. In the energy region from 0. to 50 eV, the data for

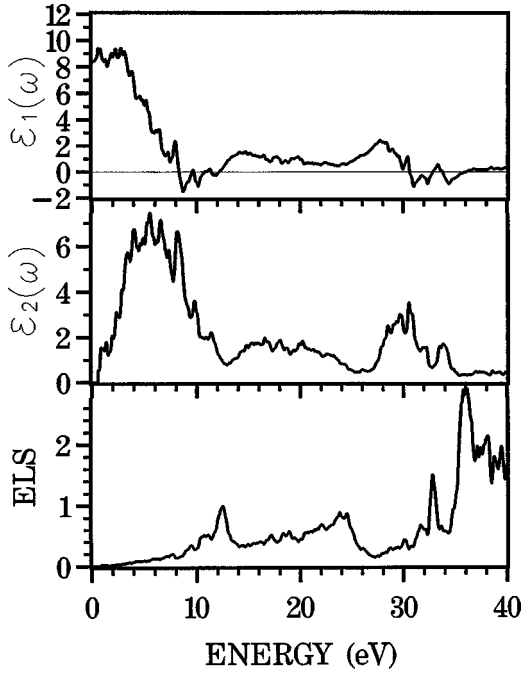

FIG. 10. Real (a) and imaginary (b) dielectric function, and energy-loss function (c) of c-Zr_3N_4.

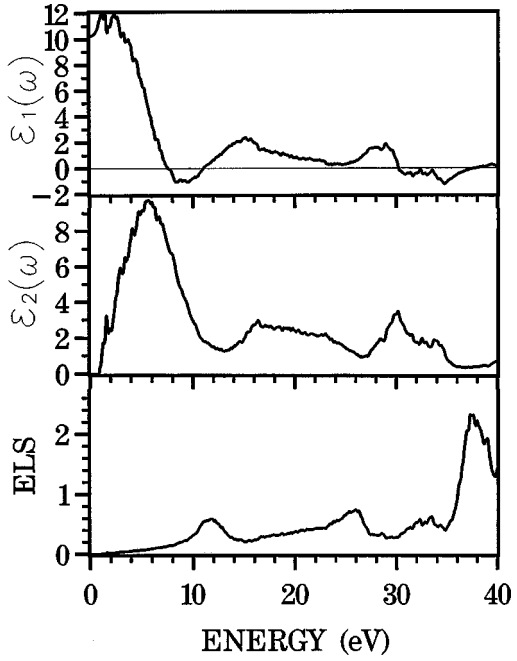

FIG. 11. Real (a) and imaginary (b) dielectric function, and energy-loss function (c) of o-Zr_3N_4.

the Zr_3N_4 sample show three plasmon peaks at 13, 22, 40 eV and a shoulder at 33 eV. The positions of these peaks agree reasonably well with the calculation for all three models. However, it has to be reminded that the data from Ref. 40 is not from direct measurements and is somewhat dependent on the model used for its conversion. These peak positions together with the experimental ones are listed in Table III.

IV. DISCUSSION

In Table III, we summarize the calculated electronic and dielectric properties of the three models for Zr_3N_4. Together with the structural data listed in Table I, a detailed comparison of the properties is possible. Calculated total energies at equilibrium geometry indicate that $Zr_3\square N_4$ has the lowest energy, and hence the most probable structure at low temperature. Comparisons with other physical observables such as the VB XPS spectra, refractive index, energy-loss functions, etc. favor the $Zr_3\square N_4$ model. This does not mean that the other structures are unlikely to exist. The o-Zr_3N_4 has been synthesized and the c-Zr_3N_4, like c-Si_3N_4 or c-Ge_3N_4, is likely to be formed under the condition of high temperature and pressure.[18] Among the three crystal models, o-Zr_3N_4 ($Zr_3\square N_4$) has the smallest (largest) volume per formula unit and hence the largest (smallest) mass density. The mass density does not scale with the Zr-N bond lengths, since Zr_{tet} in c-Zr_3N_4 actually has the shortest bond length, and hence the largest bond order values. Table IV shows that the average bond length in $Zr_3\square N_4$ and o-Zr_3N_4 are actually comparable, but that the later has a higher crystal bond order per formula unit. The high mass density and bond order in o-Zr_3N_4 is related to the extra Zr-N bond for Zr2 and Zr3 as has been pointed out in the introductory section.

The relatively large optical dielectric constants ε_0 (or equivalently, the refractive index) obtained from the optical spectral calculation deserve some comment. Among the three models, $Zr_3\square N_4$ has the smallest ε_0 value (7.82) which is in line with those implied by the optical measurements on Zr_3N_4 thin films.[9,39] The larger ε_0 values for c-Zr_3N_4 and o-Zr_3N_4 may have to do with their higher mass densities and smaller band gaps. Since the calculated ε_0 values could be affected by the size of the band gap, which is underestimated under the LDA approximation, the values for these models will be somewhat reduced. Still, these calculated ε_0 values are much larger than that of SiO_2 ($\varepsilon_0=3.90$). ZrO_2 [$n=2.15$ (Ref. 41)] and $ZrSiO_4$ [$\varepsilon_0=10.7$ to 12.6 (Ref. 42)] which are prime candidates for the development of new high dielectric oxide materials.[43,44] Thus Zr_3N_4 or the oxynitride derivative may be considered as very viable alternatives in the search for such materials.

Although we have concluded that $Zr_3\square N_4$ is the most appropriate model for Zr_3N_4, it has to be said that what we have studied is an ordered structure with one Zr vacancy in the so-called Zr_3N_4 ''supercell.'' Obviously, this is an oversimplified model and the real structure for Zr_3N_4 films is likely to be a disordered one in which the Zr vacancies are randomly distributed among the metal sublattice in the rocksalt structure. Such a disordered model will increase the entropy of the system and is more likely to exist in the real stoichiometric Zr_3N_4 thin films. However, the same relaxation of N and Zr atoms in the presence of the vacancies will occur and the electronic structure will again be an insulating one, perhaps with a slightly different band gap.

Another point worth mentioning has to do with the original idea of making $ZrN/Zr_3N_4/ZrN$ a superconductor/insulator/superconductor Josephson junction. Now we have shown that Zr_3N_4 is indeed an insulator and its lattice con-

stant matches well with that of metallic ZrN. Assuming such a multilayer device can be fabricated, the multilayer structure is no different from that of Zr_3N_4 a crystalline ZrN with alternate regions of vacancy-filled noncrystalline Zr_3N_4 with no sharp physical boundaries separating the ordered and disordered regions. Whether such a multilayered structure behaves in the same way as that of a conventional Josephson junction, say with Al_2O_3 sandwiched between superconducting Nb metal is a subject of great interest and may be worth looking into both theoretically and experimentally.

V. CONCLUSIONS

We have studied the electronic and the dielectric properties of Zr_3N_4 by first-principles density-functional calculations. The ordered defect model, $Zr_3\square N_4$, appears to be the most appropriate one for Zr_3N_4. It is shown that past calculations showing it to be that a metal was primarily due to the failure to relax the defect structure. When the atoms (especially N) relax in response to the Zr vacancy, both the local symmetry and the nature of the interatomic interactions are significantly changed and the lattice constant is slightly expanded, resulting in the insulating behavior. All three models for Zr_3N_4 are predicted to be insulators with small indirect band gaps. Comparison of calculated optical properties with the existing experimental data also favor the ordered defect model. However, accurate frequency-dependent optical data on Zr_3N_4 are not available for a more detailed comparison, signaling that further experimental efforts are urgently called for. Bulk properties calculation shows $Zr_3\square N_4$ has the highest bulk modulus. All three Zr_3N_4 model structures can be considered to be superhard materials. All three models have relatively large static dielectric constants. Such high dielectric materials can play an important role in the proper design of the next generation of microelectronic devices in which the reduced dimension requires gate insulators to have high dielectric constants. This is particularly attractive since metallic ZrN can be used as gate electrodes in MOS transistors.

ACKNOWLEDGMENT

This work was supported by U.S. Department of Energy under Grant NO. DE-FG02-84DR45170, the NEDO International grant, and partially by NSF Grant No. DMR-00162 in collaboration with NANOAM Project of EU-CODIS (Grant No. G5RD-CT-2001-00586).

[1] See for example, L. E. Toth, *The Transition Metal Carbides and Nitrides* (Academic Press, New York, 1971).
[2] S. Yamanaka, K. Hotehama, H. Kawaji, and M. Ohashi, Adv. Mater. **9**, 771 (1996).
[3] S. Yamanaka, K. Hotehama, H. Kawaji, Nature (London) **392**, 580 (1998).
[4] C. Stampfl, W. Mannstadt, R. Asashi, A. J. Freeman, Phys. Rev. B **63**, 155106 (2001).
[5] K. Schwarz, H. Ripplinger, and A. Neckel, Z. Phys. B: Condens. Matter **48**, 79 (1982).
[6] A. Neckel, Int. J. Quantum Chem. **23**, 1317 (1983).
[7] R. Juza, H. Rabenau, and I. Nitschke, Z. Anorg, Z. Anorg. Allg. Chem. **332**, 1 (1964); R. Juza, A. Godel, H. Rabenau, and W. Close, *ibid.* **329**, 136 (1964).
[8] B. O. Johansson, H. T. G. Hentzell, J. M. E. Harper, and J. J. Cuomo, J. Mater. Res. **1**, 442 (1986).
[9] R. Fix, R. G. Gordon, and D. M. Hoffman, Chem. Mater. **5**, 614 (1993).
[10] P. Prieto, A. Fernández, L. Soriano, F. Yubero, E. Elizalde, A. R. González-Elipe, and J. M. Sanz, Phys. Rev. B **51**, 17 984 (1995); J. M. Sanz, L. Soriano, P. Prieto, G. Tyuliev, C. Morant, and E. Elizalde, Thin Solid Films **332**, 209 (1998).
[11] K. Schwarz, D. S. Yee, J. J. Cuomo, and J. M. E. Harper, Phys. Rev. B **32**, 5489 (1985).
[12] K. Schwarz, A. R. Williams, J. J. Cuomo, J. M. E. Harper, and H. T. G. Hentzell, Phys. Rev. B **32**, 8312 (1985).
[13] P. Marksteiner, P. Weinberger, A. Neckel, R. Zeller, and P. H. Dederichs, J. Phys. F: Met. Phys. **16**, 1495 (1986).
[14] Jieyao Zhuang and Meichun Huang, Xiamen Daxue Xuebao, Ziran Kexueban **27**, 522 (1988).
[15] M. Lerch, E. Füglein, J. Wrba, Z. Anorg. Allg. Chem. **622**, 367 (1996).
[16] W. B. Baur and M. Lerch, Z. Anorg. Allg. Chem. **622**, 1729 (1996).
[17] W.-Y. Ching, S.-D. Mo, I. Tanaka, and M. Yoshiya, Phys. Rev. B **63**, 064102 (2001).
[18] A. Zerr, G. Miege, G. Serghiou, M. Schwarz, E. Kroke, R. Riedel, H. Fuess, P. Kroll, and R. Boehler, Nature (London) **400**, 340 (1999).
[19] H. He, T. Sekine, T. Kobayashi, H. Hirosaki, and I. Suzuki, Phys. Rev. B **62**, 11 412 (2000); T. Sekine, H. He, T. Kobayashi, M. Zhang, and F. Xu, Appl. Phys. Lett. **76**, 3706 (2000).
[20] J. Z. Jiang, K. Stahl, R. W. Berg, D. J. Frost, T. J. Zhou, and P. X. Shi, Europhys. Lett. **51**, 62 (2000).
[21] E. Soignard, M. Somayazulu, J. Dong, O. F. Sankey, and P. F. McMillan, J. Phys.: Condens. Matter **13**, 557 (2001).
[22] G. Serghiou, G. Miehe, O. Tschauner, A. Zerr, R. Boehler, J. Chem. Phys. **111**, 4659 (1999).
[23] K. Leinenweber, M. O'Keefe, M. S. Somayazulu, H. Hubert, P. F. McMillan, and G. H. Wolf, Chem.-Eur. J. **5**, 3076 (1999).
[24] M. Shemkunas, W. T. Petuskey, and G. H. Wolf, J. Am. Ceram. Soc. **85**, 101 (2002).
[25] S.-D. Mo, L. Ouyang, W. Y. Ching, I. Tanaka, Y. Koyama, and R. Riedel, Phys. Rev. Lett. **83**, 5046 (1999).
[26] W. Y. Ching, S.-D. Mo, and L. Ouyang, Phys. Rev. B **63**, 245110 (2001).
[27] W. Y. Ching, S.-D. Mo, L. Ouyang, I. Tanaka, and M. Yoshiya, Phys. Rev. B **61**, 10 609 (2000).
[28] W. Y. Ching, S.-D. Mo, Y. Chen, and P. Rulis, J. Am. Ceram. Soc. **85**, 75 (2002).
[29] W. Y. Ching, Lizhi Ouyang, and J. Gale, Phys. Rev. B **61**, 8696 (2000).
[30] Lizhi Ouyang and W. Y. Ching, J. Am. Ceram. Soc. **84**, 801 (2001).

[31] W. Y. Ching, J. Am. Ceram. Soc. **73**, 3135 (1990).
[32] Y.-N. Xu and W. Y. Ching, Phys. Rev. B **59**, 10 530 (1999); W. Y. Ching and Y.-N. Xu, *ibid.* **59**, 12 815 (1999).
[33] Y.-N. Xu, W. Y. Ching, and B. K. Brickeen, Phys. Rev. B **61**, 1817 (2000).
[34] W. Y. Ching, Y.-N. Xu, and B. K. Brickeen, Phys. Rev. B **63**, 115101 (2001).
[35] W. Y. Ching, S.-D. Mo, and L. Ouyang, Phys. Rev. B **63**, 245110 (2001).
[36] L. Ouyang, Y.-N. Xu, and W. Y. Ching, Phys. Rev. B **65**, 113110 (2002).
[37] F. D. Murnagham, Proc. Natl. Acad. Sci. U.S.A. **30**, 244 (1944).
[38] R. S. Mulliken, J. Chem. Phys. **23**, 1833 (1955).
[39] S. Camelio, T. Girardeau, L. Pichon, A. Straboni, C. Fayoux, and Ph. Guerin, J. Opt. A, Pure Appl. Opt. **2**, 442 (2000).
[40] P. Prieto, F. Yubero, E. Elizalde, and J. M. Sanz, J. Vac. Sci. Technol. A **14**, 3181 (1996).
[41] H. K. Sankur and W. Gunning, Appl. Opt. **28**, 2806 (1989).
[42] W. B. Blumenthal, *The Chemical Behavior of Zicornium* (Van Norstrand, Princeton, 1958), p. 201–219.
[43] G. D. Wilk and R. M. Wallace, Appl. Phys. Lett. **76**, 112 (2000).
[44] G. D. Wilk, R. M. Wallace, and J. M. Anthony, J. Appl. Phys. **87**, 484 (2000).